

One Copy Is All You Need: Resource-Efficient Streaming of Medical Imaging Data at Scale

Pranav Kulkarni¹, Adway Kanhere¹, Eliot Siegel¹, Paul H. Yi¹, Vishwa S. Parekh^{1*}

¹University of Maryland Medical Intelligent Imaging (UM2ii) Center, University of Maryland School of Medicine, Baltimore, MD.

*Corresponding author(s). E-mail(s): vparekh@som.umaryland.edu;

Contributing authors: pkulkarni@som.umaryland.edu; akanhere@som.umaryland.edu; esiegel@som.umaryland.edu; pyi@som.umaryland.edu;

Abstract

Large-scale medical imaging datasets have accelerated development of artificial intelligence tools for clinical decision support. However, the large size of these datasets is a bottleneck for users with limited storage and bandwidth. Many users may not even require such large datasets as AI models are often trained on lower resolution images. If users could directly download at their desired resolution, storage and bandwidth requirements would significantly decrease. However, it is impossible to anticipate every users' requirements and impractical to store the data at multiple resolutions. What if we could store images at a single resolution but send them at different ones? We propose MIST, an open-source framework to operationalize progressive resolution for streaming medical images at multiple resolutions from a single high-resolution copy. We demonstrate that MIST can dramatically reduce imaging infrastructure inefficiencies for hosting and streaming medical images by >90%, while maintaining diagnostic quality for deep learning applications.

Main

The curation of large-scale, open-source medical imaging databases has greatly accelerated the development of artificial intelligence (AI) tools for clinical decision support. The Cancer Imaging Archive (TCIA) is one of the largest cancer imaging databases with 196 open-source datasets accessed by more than 768,000 users from 216 countries with monthly downloads exceeding 140 TB [1, 2]. The large size of these datasets is a major bottleneck for users with limited computer storage capacity and internet connections (e.g., those in resource-limited areas or working remotely) [3]. For example, consider a hypothetical liver CT dataset with images of size 512x512xN

hosted in the NifTI format spanning a total storage space of 180 GB (Figure 1a). Each user working with this dataset would be required to download the entire 180 GB data to their machines for further processing. This would not only take more than 10 hours to download on a 100 Mbps internet connection, but also require a user to have 180 GB free storage space available. These large image storage sizes can quickly exhaust users' resources, especially when working with numerous datasets. Furthermore, many users may not even require such large datasets, as medical images are frequently downsampled to resolutions much lower than the original images (e.g., 224x224 for deep transfer learning); such downsampling for the referenced liver CT dataset would reduce total

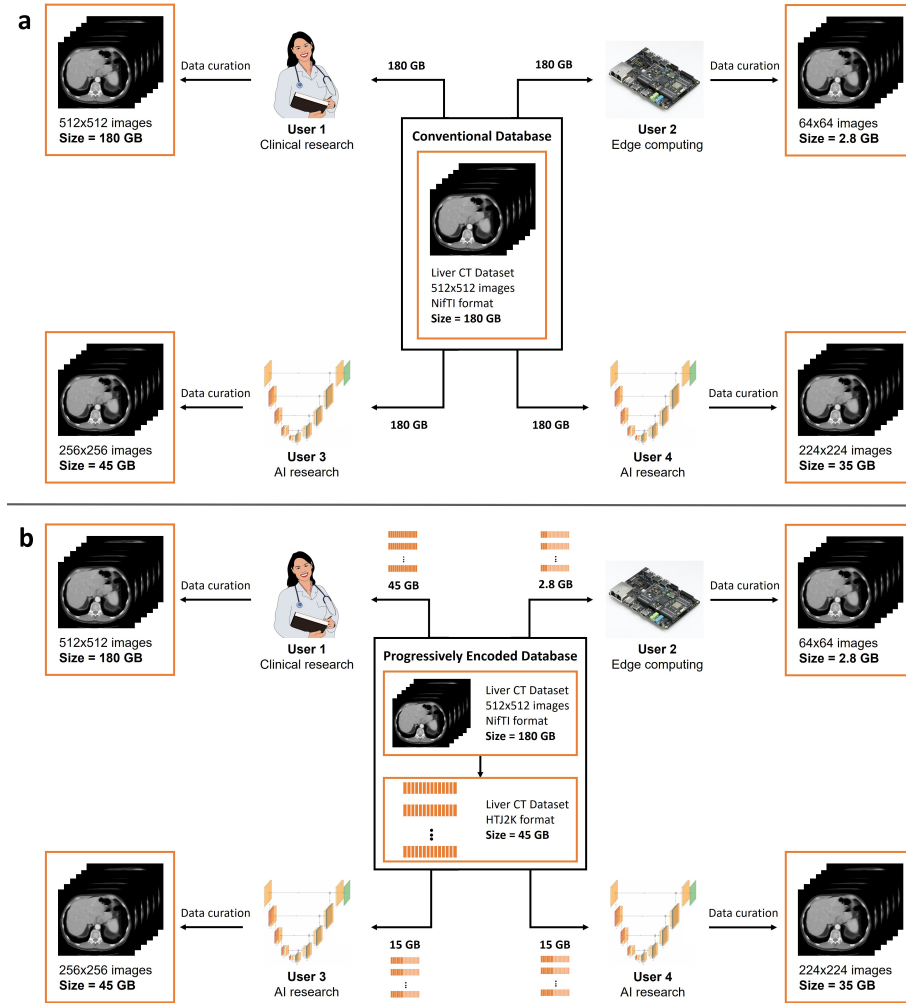


Fig. 1 a, Illustration of the conventional approach to medical imaging data curation. In this scenario, four users download a cloud-hosted liver CT dataset for different use-cases. Each use case requires a different sized image, yet the user must download the data at the baseline resolution before processing them into their desired resolutions for further analysis, resulting in inefficient use of bandwidth, storage, and compute. **b**, How can progressively encoding address the computational, network and storage inefficiencies associated with current computation infrastructures developed to host medical imaging datasets? Progressively encoding the liver CT dataset produces a storage saving of 4x for the host organization while reducing the total data transferred from the host organization by 9x. Similarly, savings in the data storage requirements for the users range from 4x–64x.

dataset size by 5x to 35 GB. If large datasets hosted by groups like the TCIA could be downloaded directly at a desired resolution, storage and bandwidth requirements for hosting and streaming medical images would dramatically decrease, and the computational resources for extra image processing would be eliminated.

These inefficiencies unfortunately scale with the number of users accessing a database. For the

example in Figure 1a, there would be an unnecessary data transfer of 450 GB in addition to increased storage requirements and image processing operations for data curation – all for just four clients in the setup. When considering that the TCIA has more than 768,000 users, the potential storage and bandwidth savings are enormous, in addition to reduced carbon footprint and impact on the environment. The ability to store and send images to users at their desired resolutions could

significantly reduce current imaging infrastructure inefficiencies by optimizing the distribution of medical images on the cloud. However, it is impossible to anticipate the requirements of every user accessing these datasets or store the data at multiple resolutions as it will result in increased cloud storage costs and unnecessary data duplication. But what if we could store the images at a single resolution but send them at different resolutions?

Progressive resolution (PR) is a promising technology capable of delivering images at multiple resolutions, even if they are stored at a single resolution [4, 5]. PR has revolutionized the way we consume media content over the internet, addressing similar infrastructural inefficiencies associated with hosting and streaming consumer media. The core concept behind PR has enabled streaming platforms like Netflix to optimize delivery of media at scale, by streaming content at different resolutions depending on individual users’ devices (e.g., iPhone vs. 4K TV) and network speeds from a single high-resolution copy [6]. However, the computational overhead of PR codecs has held back its adoption in medical imaging beyond niche web-based applications [4]. PR has received recent interest within the medical imaging community with the proposed integration of High-Throughput JPEG 2000 (HTJ2K) [7, 8] – a state-of-the-art lossless PR codec that addresses its predecessors’ drawbacks – into DICOMWeb, the industry standard for web-based medical imaging [9]. Furthermore, HTJ2K has been adopted by the recently launched Amazon Web Services’ HealthLake Imaging as part of their toolkit for encoding medical images for rapid retrieval [10]. Briefly, HTJ2K encodes images into a series of progressive decompositions, each with an increasing level of detail, and enables them to be decoded into different resolutions by selecting different subset of bytes (i.e., partial bytestreams). In contrast, vast majority of image codecs (e.g., JPEG) sequentially encode an image from the top-left to the bottom-right pixels; this sequential encoding prevents images from being decoded from a partial bytestream in the same way that HTJ2K allows (Figure 2).

Despite widespread and growing enthusiasm for the integration of HTJ2K in medical imaging data standards, there is a critical unmet need to operationalize PR for streaming medical imaging,

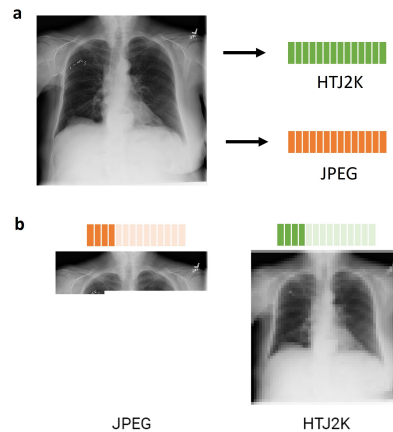


Fig. 2 **a**, A chest X-Ray image encoded using JPEG (sequential) and HTJ2K (progressive) encoders. **b**, Decoding the chest X-ray image using partial bytestreams from both the JPEG and HTJ2K encodings. The JPEG decoded image was a partially visible image (left) whereas the HTJ2K decoded image was visible, albeit lower in resolution (right).

with current software difficult to use and lacking specificity for medical imaging data management. To that end, we propose the Medical Image Streaming Toolkit (MIST), an open-source framework that operationalizes PR for medical imaging data by progressively encoding and streaming medical imaging datasets. MIST is built on the scientific premise that PR can 1) dramatically reduce medical image data infrastructure costs by reducing storage and data transfer bandwidth requirements and 2) improve image data useability by making it more practical for users to download this data, even with low storage or slow internet connections (Figure 1b). In this work, we aim to demonstrate that MIST can dramatically reduce medical image data infrastructure requirements for hosting and streaming datasets while maintaining diagnostic image quality and information for deep learning analyses and applications.

Results

We developed MIST as an end-to-end toolkit with the capability to progressively encode, decode, and stream medical imaging data over the internet and consisting of two major components: 1) progressive encoder-decoder framework and 2) progressive streaming framework, as shown in Figure 3.

Progressive Encoder-Decoder Framework

The progressive encoding technology provides the basis for storing images at a single resolution with the ability to send the images at different resolutions as requested by the user. The MIST framework utilizes the HTJ2K codec to enable progressive encode-decode capabilities, achieve a high compression ratio, and enable rapid access to lower resolution versions of the original high-resolution copy. MIST’s progressive encoder-decoder framework’s builds on the capabilities of HTJ2K through two important capabilities: 1) multi-format encode-decode capability to enable users to progressively encode both 2D and 3D medical imaging data acquired in different imaging formats (e.g., DICOM, NifTI, PNG, etc.) across various imaging modalities (CT, MRI, X-ray) and 2) stream optimization map to enable users to download images at their desired resolutions directly from the high-resolution copy.

We evaluated the progressive encoder-decoder framework using three datasets sourced from different repositories. The first dataset is a multi-parametric brain MRI dataset sourced from the UPENN-GBM collection on TCIA [2, 11] and comprising of 3,301 mpMRI studies in the DICOM format, encompassing a total of 133.37 GB of storage space. The second dataset is a liver CT dataset, sourced from the MSD archive, consisting of 131 3D CT volumes in the NifTI format, encompassing a total space of 18.34 GB [12]. The third dataset is the NIH Chest X-Ray dataset [13] with 112,120 frontal-view chest X-rays in the PNG format from 30,805 unique patients, encompassing a total of 42.39 GB of storage space. All three datasets were first encoded using MIST’s progressive encoder, followed by lossless decoding of each of the datasets back to their original resolution. We measured the framework’s encoding efficiency across all three imaging formats by comparing the storage space required to host the original dataset and the progressively encoded dataset. Furthermore, we quantitatively evaluated MIST’s lossless decoding capability by measuring the structural similarity index measure (SSIM) and mean absolute deviation (MAD) between the reconstructed images against the original images across all three datasets. As shown in Table 1, the progressively

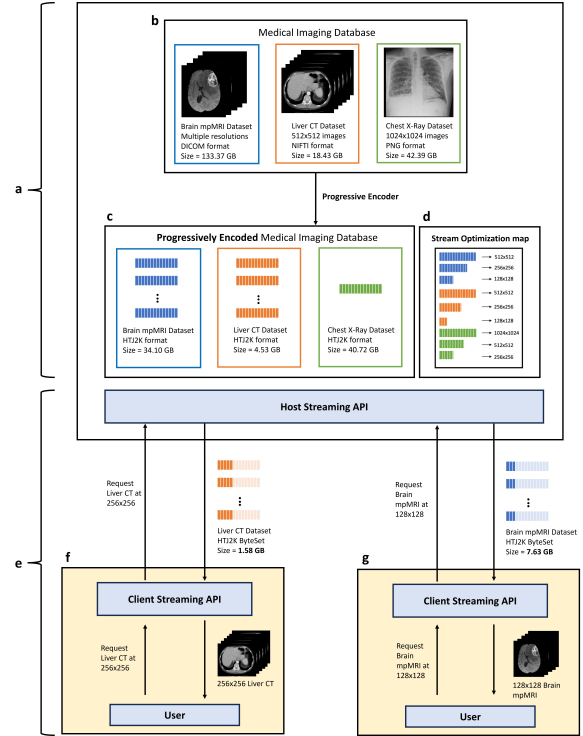


Fig. 3 Illustration of the Medical Image Streaming Toolkit (MIST). **a**, The progressive encoder-decoder framework encodes the medical images **(b)** into progressively encoded HTJ2K images **(c)** and generates a stream optimization map **(d)** between different byte subsets and image resolutions. **e**, The progressive streaming framework enables the users **(f-g)** to request images at their desired resolutions by determining the appropriate partial bytestream and decoding them into desired imaging formats for further analysis. Using MIST, the left user **(f)** was able to download the entire liver data in 1.58 GB (as opposed to 18.43 GB) and the right user **(g)** was able to download the entire brain mpMRI data in 7.63 GB (as opposed to 133.73 GB) resulting in 15x bandwidth and storage savings.

encoded datasets produced excellent encoding efficiency, compressing the brain mpMRI dataset by 74.43% (3.91x) from 133.37 GB down to 34.10 GB, liver CT dataset by 75.28% (4.07x) from 18.43 GB down to 4.53 GB, and the NIH Chest X-Ray dataset by 3.95% (1.04x) from 42.39 GB to 40.72 GB. Furthermore, the images reconstructed back to original resolution using the progressive decoder produced a mean SSIM of 1.00 and MAD of 0.00 across all datasets.

Table 1 Summary of the quantitative evaluation of MIST’s encoding, decoding, and streaming efficiency, compared to the conventional approach. For the host, MIST’s encoding efficiency and lossless decoding efficiency is measured. For the client, MIST’s streaming and lossy decoding efficiency is measured at the user’s requested resolution. Quantitative metrics reported as Mean \pm SD.

Dataset	NIH Chest X-Ray	MSD Liver	UPENN-GBM
Modality	X-ray	CT	mpMRI
Format	PNG	NifTI	DICOM
Compression	Lossless	Lossless	-
Storage Size (GB)			
Original	42.39	18.34	133.37
HTJ2K	40.72 (-3.95%)	4.53 (-75.28%)	34.10 (-74.43%)
Quantitative Metrics			
SSIM	1.000 \pm 0.0000	0.999 \pm 0.0002	1.000 \pm 0.0001
MAD	0.000 \pm 0.0000	0.001 \pm 0.0001	0.001 \pm 0.0002
Requested Resolution			
	224x224	256x256	128x128
Data Transmitted (GB)			
Original	42.39	18.34	133.37
HTJ2K	3.53 (-91.68%)	1.58 (-91.38%)	7.63 (-94.28 %)
Quantitative Metrics			
SSIM	0.971 \pm 0.0087	0.959 \pm 0.0150	0.968 \pm 0.0590
MAD	0.011 \pm 0.0022	0.010 \pm 0.0038	0.011 \pm 0.0137

Progressive Streaming Framework

The progressive streaming framework provides open-source tools and APIs that allow users to interface with MIST’s progressively encoded imaging database and download datasets at desired resolutions, consisting of a host API and a client API, to facilitate this interaction. The host API interfaces with the progressively encoded imaging database and the stream optimization map database to splice and stream partial bytestreams that are sufficient to reconstruct the images to resolution requested by the user. If the requested resolution is not available, MIST automatically transmits the partial bytestream corresponding to the closest sub-resolution available. This ability to splice and stream partial bytestreams is vital component behind MIST’s data transmission efficiency as currently available software offerings that utilize PR are not equipped with the capability to splice, transmit, and decode partial bytestreams. On the other hand, the client API will enable the user to request and reconstruct the partial bytestreams directly into imaging formats like NifTI, which can be seamlessly utilized by various open-source tools including MONAI and nnUNet [14–16] for subsequent AI modeling and analysis. In this study, we evaluate 1) the ability of the progressive streaming framework to reduce the bandwidth and storage requirements for streaming large-scale datasets over the network and 2) compare the performance of AI models developed using progressively streamed data at

the desired resolution with AI models developed using conventionally downsampled data at the same resolution.

We used the progressively encoded NIH Chest X-ray, MSD liver CT, and UPENN-GBM brain mpMRI datasets from the previous experiment to request and reconstruct sub-resolution images from the partial bytestreams for each dataset. Furthermore, we repeated the quantitative analysis to measure the SSIM and MAD comparing the reconstructed sub-resolution images to the conventional approach (i.e., downsampling the original dataset). In short, the NIH Chest X-ray dataset was requested at a resolution of 224x224. Since this resolution was unavailable in the stream optimization map, MIST automatically streamed 256x256 images, i.e., the closest sub-resolution available. The liver CT dataset was requested, streamed, and decoded at a resolution of 256x256 since the requested resolution was available. Similarly, the brain mpMRI dataset was requested, streamed, and decoded at a resolution of 128x128. As shown in Table 1, the NIH Chest X-ray, liver CT, and brain mpMRI datasets were streamed using 3.53 GB, 1.58 GB, and 7.63 GB of data, i.e., 91.68%, 91.38%, and 94.28% less data transmitted compared to the original dataset, respectively. In aggregate, MIST dramatically reduced the amount of data transmitted over the network by 93.44% (15.24x) from 194.10 GB to 12.74 GB. Furthermore, the mean SSIM between the conventionally downsampled and progressively streamed datasets was 0.97, 0.96, and 0.97 for the NIH

Table 2 Summary of the performance of deep learning classification and segmentation models trained on conventionally downsampled and progressively streamed medical imaging datasets. Mean AUC scores reported with 95% C.I. in brackets. Dice scores reported as Mean \pm SD.

	Internal Test Set	External Test Set
Classification		
Dataset	NIH Chest X-Ray	MIMIC-CXR-JPG
Format	PNG	JPEG
Sample Size, N	22,330	377,110
Conventionally Downsampled Model		
Loss	0.1502	0.3697
Mean AUC	0.8135 [0.8063, 0.8199]	0.7400 [0.7386, 0.7414]
p-value	-	-
Progressively Streamed Model		
Loss	0.1498	0.3836
Mean AUC	0.8166 [0.8090, 0.8242]	0.7391 [0.7375, 0.7406]
p-value	0.37	0.22
Segmentation		
Dataset	MSD Liver	BTCV
Format	NifTI	NifTI
Sample Size, N	25	30
Conventionally Downsampled Model		
Dice Score	0.9451 \pm 0.0171	0.8705 \pm 0.1106
p-value	-	-
Progressively Streamed Model		
Dice Score	0.9541 \pm 0.0093	0.8447 \pm 0.1610
p-value	<0.001	0.06

Chest X-Ray, liver CT, and brain mpMRI dataset respectively with a MAD of 0.01 across all three datasets.

The primary goal of developing the progressive streaming framework is to reduce computational infrastructure and network bandwidth costs for researchers training and validating AI models on large datasets. Thus, it is important to evaluate the performance of AI models trained on progressively streamed datasets in comparison to AI models trained using original datasets. We compared the performance of deep learning classification and segmentation models trained using progressively streamed NIH Chest X-ray and liver CT datasets with models trained using conventionally downsampled datasets.

Deep Learning Classification

We trained two deep learning classification models using transfer learning on the NIH Chest X-Ray dataset. The first model was trained on the original PNG images and the second model was trained on the progressively streamed images. Both models were then evaluated on the original internal test set ($n = 22,330$) and externally tested on the MIMIC-CXR-JPG dataset ($n = 377,110$) [17, 18]. The performance of both models was measured by the binary cross-entropy (BCE)

loss and the mean area under the receiver operating characteristic curve (AUC) across all observed disease labels. As shown in Table 2, we observe that the classification model trained using progressively streamed images demonstrated similar performance across the internal and external test sets with a mean AUC of 0.82 ($p = 0.37$) and 0.74 ($p = 0.22$) respectively, when compared to the model trained using conventionally downsampled images.

Deep Learning Segmentation

We trained two deep learning 3D segmentation models on the MSD liver CT dataset. The first model was trained on the original NifTI volumes and the second model was trained on progressively streamed volumes. Both models were similarly evaluated on the original internal test set ($n = 25$) with external testing on the BTCV dataset ($n = 30$) [19]. The performance of both models was measured by the mean dice score. As shown in Table 2, we observe that the segmentation model trained using progressively streamed volumes demonstrated similar, if not better, performance across the internal test set with a mean dice score of 0.95 ($p < 0.001$). On the external BTCV test set, we observed a slight, albeit non-significant, degradation to the performance of

the model trained using progressively streamed volumes with a mean dice score of 0.85 ($p = 0.06$).

Discussion

Our results demonstrate that the scientific premise behind MIST holds true with concrete results from three large-scale real-world medical imaging datasets – i.e., MIST can efficiently compress and encode, stream, and decode medical imaging data across different formats, modalities, and body parts, while maintaining diagnostic quality for deep learning applications. We show that MIST has the potential to dramatically reduce medical image data infrastructure costs by reducing storage and bandwidth requirements to host and stream data over the network, while making large medical imaging datasets more accessible to users with limited storage and slow internet connections. More importantly, by reducing the network and computational overhead of data transmission and image preprocessing (e.g., down-sampling) without affecting further downstream applications for medical images, MIST has the potential to significantly reduce the carbon footprint and environmental impact of large-scale medical image data infrastructure.

In stark contrast to currently available software offerings and toolkits, MIST provides two significant improvements – owing to its high-throughput and resource-efficiency. First, MIST’s progressive encoder enables users to progressively encode both 2D and 3D medical imaging data in different imaging formats (PNG, DICOM, NifTI, etc.) across various modalities (MRI, CT, X-ray, etc.). In contrast, current progressive encoding solutions only support encoding of raw DICOM images [10] – a major limiting factor due to the prominence of other imaging formats such as NifTI in further downstream analyses and applications [12, 14, 15]. Finally, MIST has the capability to splice, stream, and decode partial bytestreams using the stream optimization map. Since the progressive encoding technology was not developed to transmit partial bytestream but to deliver the complete bytestream with the goal of enhancing the user experience in case of network interruptions (e.g., for Netflix movie streaming), current tools lack the specificity to decode partial bytestreams nor do they generate or store an

encoding dictionary that maps different byte subsets to different image resolutions, which is a key technical requirement for reconstructing images from partial bytestreams. Furthermore, MIST has the capability to decode the partial bytestream directly into imaging formats such as NifTI for further downstream applications – a missing link between current software offerings and successfully operationalizing PR for medical imaging.

Unfortunately, at this stage of development, MIST is not devoid of its own limitations that are an impediment to its deployment in current large-scale medical image data infrastructures. Due to current progressive encoder-decoder tools lacking the specificity required for medical images, imaging data stored with high-precision floating point intensities suffer from a minimal loss of quality during the encoding process – 0.001 MAD for the liver CT and brain mpMRI datasets. While our results show that this loss of quality does not negatively impact further downstream deep learning applications, it is crucial to address this limitation prior to MIST’s deployment. Promisingly, the HTJ2K codec supports encoding floating point data despite the limitations of current encoding frameworks [4, 8]. On the other hand, 3D medical imaging data (e.g., NifTI) poses a challenge to integrating MIST in current cloud-based solutions. Since the HTJ2K codec only supports encoding 2D data, there is an additional overhead to correctly process 3D data for progressive encoding-decoding. However, in our prior work, we have showed that even with this additional overhead, encoding, streaming, and decoding of 3D imaging data using HTJ2K is significantly faster and more resource-efficient than NifTI encoded volumes [20]. Finally, future work is warranted to extensively validate the MIST framework for not just deep learning applications, but also for further downstream analyses (e.g. radiomics) and clinical use-cases through in-depth diagnostic equivalence reader studies with board-certified radiologists to evaluate.

Despite current limitations, our results demonstrate that MIST provides substantial improvements compared to current software solutions and has the potential to overhaul large-scale medical imaging data infrastructures. Returning back to our hypothetical four-node liver CT set up in Figure 1a, if we were to use MIST to progressively encode the entire dataset and then only stream the

partial bytestream required by each user for their particular use-case, we would dramatically reduce the bandwidth, storage, and compute utilization across all users without additional computational overhead. In addition, the lossless compression provided by HTJ2K would also reduce the storage requirement for the hosting organization (e.g., TCIA). As shown in Figure 1b, the host organization would reduce their overall storage by 4x from 180 GB to 45 GB and their total data transmission by 9x from 720 GB to 77.8 GB using MIST. Similarly, all users would observe tremendous savings in terms of storage space required and bandwidth used to download the data (savings between 4x–64x), eliminating additional computational overhead required to downsample the imaging data. As cloud-based solutions for medical imaging data infrastructure gain popularity, MIST presents an open-source, resource-efficient, and scalable framework to meet the critically unmet need to dramatically reduce infrastructural inefficiencies associated with hosting and streaming medical images over the Internet.

Methods

High-Throughput JPEG 2000 (HTJ2K)

High-Throughput JPEG 2000 (HTJ2K) is an extension to the existing JPEG 2000 (J2K) codec, that – unlike the original JPEG standard – enables faster decoding, higher quality, lossless encoding with high scalability, and progressive decoding of images [4, 8]. The HTJ2K codec utilizes new lightweight and efficient block-coder algorithm that yields up to 10-30x increase in throughput for lossless coding and a 6-10% increase in efficiency when compared to J2K [7]. Furthermore, HTJ2K’s lower computational complexity and support for parallelism results in a throughput on par, or even better, than the heavily optimized original JPEG standard in single and multi-threaded applications [8].

In short, imaging data is progressively encoded using lossless HTJ2K as N decompositions, i.e., subsets of the bytestream, each with a native resolution as a factor of 2^N of the full image resolution. The native resolution of a decomposition refers to the proportion of pixels of the full resolution image transmitted prior to any interpolation.

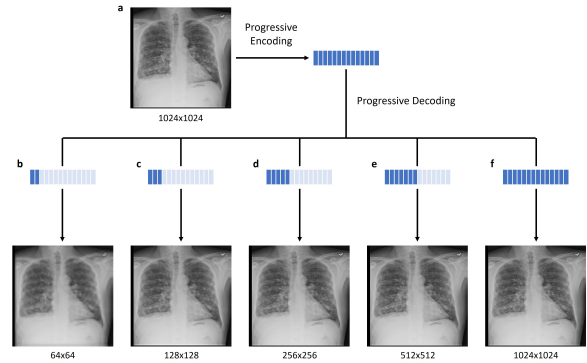


Fig. 4 Illustration of the ability of the HTJ2K codec for encoding a chest X-ray dataset (a) and subsequently decoding the dataset at different resolutions by selecting different subsets of the bytestream i.e., partial bytestreams (b-f).

Unlike the sequential streams of the original JPEG standard, HTJ2K streams are transmitted as a sequence of these N decompositions. For example, a 2D chest X-ray with a resolution of 1024x1024 can be progressively encoded as 5 decompositions with native resolutions 64x64, 128x128, 256x256, 512x512, and 1024x1024 (visualized in Figure 4). This allows HTJ2K to both achieve a high compression ratio and enable rapid access to lower resolution versions of the original high-resolution image, thus minimizing data duplication.

Medical Image Streaming Toolkit (MIST)

The Medical Imaging Streaming Toolkit (MIST) is an end-to-end toolkit with the capability to progressively encode, decode, and stream medical imaging data over the network, comprising of two major components: 1) progressive encoder-decoder framework, and 2) progressive streaming framework, as previously shown in Figure 3. Our implementation of MIST is open-source and available on GitHub [21], with source code to replicate our study in a separate repository [22].

Progressive Encoder-Decoder Framework

The progressive encoder-decoder framework provides two important capabilities: 1) multi-format encode-decode and 2) stream optimization map. MIST’s multi-format encode-decode capability

enables users to progressively encode both 2D and 3D medical imaging data acquired in different imaging formats (e.g., DICOM, NifTI, PNG, JPEG, etc.) across any imaging modalities (CT, MRI, X-Rays, etc.) as a series of N decompositions, as shown in Figure 4. We integrate OpenJPH, an open-source implementation of the HTJ2K codec [23], within MIST to interface with HTJ2K capabilities.

Correctly encoding imaging data across multiple formats and accounting for variations within each format is critical to operationalizing PR for medical imaging. In general, all imaging data is encoded by OpenJPH as lossless with 64x64 block size, N decompositions (determined by Equation 1), and tile-part markers to identify location of each decomposition (i.e. sub-resolution) within the complete bytestream. While encoding 2D imaging data is straightforward, there is an additional overhead to correctly encode 3D imaging data. For example, the NifTI format encodes the entire 3D volume within a single file. When encoding NifTI data, MIST splits and progressively encodes each slice separately as a 2D image. Not only does this require additional preprocessing during the encoding process, but also during the decoding process as individual slices must be tracked, reconstructed, and restitched to yield the final 3D volume. Fortunately, this process is relatively straightforward as MIST strips DICOM and NifTI metadata prior to encoding and tracks all relevant information within a manifest file, and enables MIST to achieve a higher compression ratio than NifTI.

$$N = \left\lceil \log_2 \left(\frac{\min(X, Y)}{\alpha} \right) \right\rceil \quad (1)$$

where N is the number of decompositions to encode, (X, Y) is the resolution of an image, and α is lower bound for the resolution of the first decomposition (i.e., the smallest sub-resolution) such that it exceeds α . In our study, we arbitrarily set $\alpha = 32$.

Due to limitations in current open source HTJ2K encode-decode frameworks, there is a minor loss of image fidelity during progressive encoding. For example, the OpenJPH library is written in C++ and only supports encoding and decoding at 16-bit precision for unsigned integers (i.e. pixel values ranging from 0 to 65,535) [23].

However, due to limitations in integrating OpenJPH with Python, we were only able to maintain 8-bit precision (i.e. pixel values ranging for 0 to 255) [24]. Consequently, prior to encoding, all imaging data is resampled to fit within the $[0, 255]$ range and original pixel value range is stored in the manifest file. During decoding, the reconstructed image is subsequently resampled back to the original data’s pixel value range. While this severely limits the fidelity of our current setup, for future work, we have a two-fold plan of action: 1) Extend precision to 16-bit in current setup, and 2) Implement an end-to-end integration of OpenJPH in Python with direct encode-decode capabilities to leverage HTJ2K’s 16-bit floating point precision (i.e. values ranging from -65,504 to 65,504). Our implementation of OpenJPH’s Python integration is open-source and available on GitHub [25].

After imaging data is encoded, a stream optimization map is generated. In short, the stream optimization map enables rapid sub-resolution access by mapping the sub-resolution to the partial bytestream necessary to decode the imaging data at the sub-resolution (e.g., reconstructing image at 256x256 resolution requires the first 12 KB of the complete 354 KB bytestream). This map is generated by locating each tile-part marker in the bytestream (identified by bytes 0xFF90 and 0xFFD9 [26]), emphasizing the significance of including tile-part markers during the encoding process. Similarly, each sub-resolution is automatically calculated as a factor of 2^N , where N is the number of decompositions (e.g., a 1024x1024 image consisting of 5 decompositions has sub-resolutions 64x64, 128x128, etc.).

Progressive Streaming Framework

The progressive streaming framework provides two interfaces to interact with the progressive imaging database generated by the progressive encoder-decoder framework: 1) host API, and 2) client API. In short, both APIs function together to enable users to request imaging data at their desired resolutions. The host API interfaces with the imaging database to splice (i.e., truncate) and stream partial bytestreams to the user using the stream optimization map. The client API uses these partial bytestream to decode and reconstruct medical imaging data at the user’s requested resolution. If the user’s

requested resolution is not available in the stream optimization map, the client API requests the closest sub-resolution. This enables MIST to account for all possible applications, while providing the substantial improvements of streaming partial bytestreams. Furthermore, the client API handles all necessary conversions based on the user’s request into formats such as PNG, JPEG, DICOM, NifTI, etc. For example, the client API can automatically reconstruct and restitch imaging data into NifTI (including adapting all affine transformations to ensure pixel coordinates map correctly to real-world coordinates – a crucial step to maintain scale of anatomical parts for clinical use-cases).

Datasets

NIH Chest X-Ray 14

The NIH Chest X-Ray dataset [13] consists of 14 disease labels with $n = 112,120$ frontal-view chest x-rays from 30,805 unique patients, encompassing a total size of 42.39 GB. All images within the dataset have a fixed 1024x1024 resolution and are encoded in PNG (lossless) format.

MSD Liver

The Medical Segmentation Decathlon (MSD) dataset is a collection of 2,633 CT and MRI studies spanning 10 body parts [12]. We selected the liver segmentation subset of the MSD dataset, consisting of $n = 131$ CT studies in the NifTI format with a fixed resolution of 512x512xN (i.e., N is the varying number of slices in each volume), encompassing a total size of 18.34 GB.

UPENN-GBM

The UPENN-GBM dataset is an extensive collection hosted on TCIA focusing on glioblastoma patients and comprising of multiparametric MRI (mpMRI) studies, patient demographics, clinical outcomes, and more [1, 11]. For our study, we selected the brain mpMRI subset of the collection, containing $n = 3,301$ studies from 630 unique patients in the raw DICOM format (i.e., implicit VR endian) consisting of T1-pre, T1-post, FLAIR, and T2-weighted sequences acquired at different resolutions ranging from 128x128 to 512x512, encompassing a total of 133.7 GB of storage space.

MIMIC-CXR-JPG

The MIMIC-CXR-JPG dataset [17, 18] consists of 14 disease labels, seven of which are shared with the NIH Chest X-Ray dataset, with $n = 377,110$ frontal and lateral chest x-rays from 65,379 unique patients. All images within the dataset are encoded in JPEG format with resolutions ranging from 1470x1461 to 4280x3520. For our study, only the seven disease labels shared with the NIH Chest X-Ray dataset – i.e., atelectasis, cardiomegaly, consolidation, edema, pleural effusion, pneumonia, and pneumothorax – were considered. To handle uncertain labels in the dataset, we chose the U-Zeros approach i.e. all uncertain labels were treated as negatives.

BTCV

The Beyond The Cranial Vault (BTCV) dataset [19] is a multi-organ abdominal CT dataset consisting of $n = 30$ studies in the NifTI format with a fixed resolution of 512x512xN and 13 segmentation labels for each volume. For our study, only the liver segmentation masks for each volume were used.

Experimental Design

In our study, we evaluate MIST across each of its capabilities, from progressive encoding-decoding to its downstream applications in deep learning, across different modalities and body parts, using three datasets: 1) NIH Chest X-Ray dataset, 2) MSD Liver CT dataset, and 3) UPENN-GBM Brain mpMRI dataset.

Progressive Encoding-Decoding

We validate MIST’s progressive encoder-decoder framework by progressively encoding all three datasets, followed by losslessly decoding each of the datasets back to their original resolution. We measured the framework’s encoding efficiency across all three datasets by comparing the storage space required to host the original dataset and the progressively encoded dataset. Furthermore, we quantitatively evaluate MIST’s lossless decoding capability by measuring the structural similarity index measure (SSIM), as described in Wang et al. [27], and the mean absolute deviation (MAD),

as described in Equation 2, between the reconstructed images and the original images across all three datasets.

$$\text{MAD} = \frac{1}{XY} \sum_{i=1}^X \sum_{j=1}^Y |M_{ij} - M'_{ij}| \quad (2)$$

where M, M' are two 2D images with resolution (X, Y) .

Progressive Streaming

We validate MIST’s progressive streaming framework by analyzing its effect on deep learning classification and segmentation – two foundational downstream use-cases for medical imaging data. In our study, for both tasks, we train two distinct deep learning models using fixed architecture and hyperparameters with the first model trained on progressively streamed images, while the second model is trained on conventionally downsampled images. Both models are subsequently evaluated on a held-out internal test set and an external test set (each test set’s original format is used for testing).

Deep Learning Classification: We used a multi-label DenseNet121 model architecture [28], initialized with ImageNet weights, and used transfer learning to train the model on the NIH Chest X-Ray dataset. The dataset was randomly divided into training (70%, $n = 78,571$), validation (10%, $n = 11,219$), and testing (20%, $n = 22,330$) splits, while ensuring no patient appears in more than one split. For preprocessing, all images were downsampled to 224x224 resolution, normalized between 0 and 1, and data augmentation (e.g., random crop, rotation, contrast, etc.) was used. Both models were trained, using a batch size of 64, in a two-fold manner: 1) The new classification heads were warmed up, while the rest of the model weights remained frozen, using transfer learning for 15 epochs with a learning rate of 5e-2. 2) The best performing model from the first round was chosen and fine-tuned after unfreezing all model weights for 50 epochs with a learning rate of 5e-4 and early stopping after 10 epochs with no improvement. The best models were chosen by the minimum BCE loss on the validation set. After the training phase, both models were then evaluated on the held-out internal NIH Chest X-Ray test set ($n = 22,330$) and the external MIMIC-CXR-JPG ($n = 377,110$) to measure the

BCE loss and mean AUC scores. In a multi-label scenario, the mean AUC score is the macro average of the AUC for each disease label. For the NIH Chest X-Ray test set, both metrics were measured on the complete set of 14 disease labels, while for the MIMIC-CXR-JPG dataset, only the seven common disease labels were used. We statistically compared the mean AUC from each test set across both models using bootstrapping and t-test. Statistical significance was defined as $p < 0.05$.

Deep Learning Segmentation: We used a 3D-UNet [29] using the MONAI framework [14] for the segmentation of liver using the MSD Liver CT dataset. The model architecture consisted of five two-convolutional residual units with down/up-sampling by a factor of 2 at each unit. The dataset was randomly divided into training ($n = 106$) and validation/testing ($n = 25$). For this study, all liver tumor annotations were discarded, maintaining annotations only for the organ. For preprocessing, all volumes were resized to 256x256x128 with constant voxel spacing of (1.5, 1.5, 2), intensity values were normalized between 0 and 1, and data augmentation was used. Random foreground patches of size 128x128x32 were extracted from each volume such that the center voxel of each patch belonged to either the foreground or background class. Prior to training, the models were initialized using LeCun’s method [30]. Both models were trained for 500 epochs with batch size of 2, an initial learning rate of 1e-4, and cosine annealing learning rate scheduler [31]. The best models were chosen by the highest mean Dice score on the validation set. After the training phase, both models were evaluated on the internal MSD Liver test set ($n = 25$) and the external BTCV test set ($n = 30$) to measure the mean Dice score between the ground truth segmentation and the model’s prediction segmentation. We statistically compared the mean Dice scores from each test set across both models using a two-tailed paired t-test. Statistical significance was also defined as $p < 0.05$. While the sample sizes for segmentation are small compared to classification, power analysis shows us that a sample size of $n = 25$ is sufficient for a two-tailed paired t-test with significance level of $p < 0.05$, with an effect size of 0.8 (Cohen’s d for large effect sizes), to ensure at least 80% statistical power.

References

- [1] Eary, J.F.: The Cancer Imaging Archive (TCIA). <https://deainfo.nci.nih.gov/advisory/fac/0222/Eary.pdf>. (Accessed on 06/26/2023) (2022)
- [2] Clark, K., Vendt, B., Smith, K., Freymann, J., Kirby, J., Koppel, P., Moore, S., Phillips, S., Maffitt, D., Pringle, M., *et al.*: The cancer imaging archive (tcia): maintaining and operating a public information repository. *Journal of digital imaging* **26**, 1045–1057 (2013)
- [3] Douthit, N., Kiv, S., Dwolatzky, T., Biswas, S.: Exposing some important barriers to health care access in the rural usa. *Public health* **129**(6), 611–620 (2015)
- [4] Foos, D.H., Muka, E., Slone, R.M., Erickson, B.J., Flynn, M.J., Clunie, D.A., Hildebrand, L., Kohm, K.S., Young, S.S.: Jpeg 2000 compression of medical imagery. In: *Medical Imaging 2000: PACS Design and Evaluation: Engineering and Clinical Issues*, vol. 3980, pp. 85–96 (2000). SPIE
- [5] Munteanu, A., Cornelis, J., Cristea, P.: Wavelet lossy and lossless image compression techniques—use of the lifting scheme. *Articles Digital Signal Processing Laboratory* (1998)
- [6] Bentaleb, A., Taani, B., Begen, A.C., Timmerer, C., Zimmermann, R.: A survey on bitrate adaptation schemes for streaming media over http. *IEEE Communications Surveys & Tutorials* **21**(1), 562–585 (2018)
- [7] Taubman, D., Naman, A., Mathew, R., Smith, M., Watanabe, O., Lemieux, P.-A.: High Throughput JPEG 2000 (HTJ2K) and the JPH file format: a primer. <https://ds.jpeg.org/whitepapers/jpeg-htj2k-whitepaper.pdf> (2020)
- [8] Taubman, D., Naman, A., Mathew, R., Smith, M., Watanabe, O.: High throughput JPEG 2000 (HTJ2K): Algorithm, performance and potential. *International Telecommunications Union (ITU)*, 15444–15 (2019)
- [9] Hafey, C., Wallace, B.: HTJ2K Transfer Syntax Support. <https://www.dicomstandard.org/docs/librariesprovider2/default-document-library/htj2k-transfer-syntax-support.docx> (2022)
- [10] Amazon Healthlake. <https://aws.amazon.com/healthlake/>. Accessed: 2023-02-27
- [11] Bakas, S., Sako, C., Akbari, H., Bilello, M., Sotiras, A., Shukla, G., Rudie, J.D., Santamaría, N.F., Kazerooni, A.F., Pati, S., *et al.*: The university of pennsylvania glioblastoma (upenn-gbm) cohort: Advanced mri, clinical, genomics, & radiomics. *Scientific data* **9**(1), 453 (2022)
- [12] Antonelli, M., Reinke, A., Bakas, S., Farahani, K., Kopp-Schneider, A., Landman, B.A., Litjens, G., Menze, B., Ronneberger, O., Summers, R.M., *et al.*: The medical segmentation decathlon. *Nature communications* **13**(1), 4128 (2022)
- [13] Wang, X., Peng, Y., Lu, L., Lu, Z., Bagheri, M., Summers, R.M.: Chestx-ray8: Hospital-scale chest x-ray database and benchmarks on weakly-supervised classification and localization of common thorax diseases. In: *Proceedings of the IEEE Conference on Computer Vision and Pattern Recognition*, pp. 2097–2106 (2017)
- [14] Cardoso, M.J., Li, W., Brown, R., Ma, N., Kerfoot, E., Wang, Y., Murrey, B., Myronenko, A., Zhao, C., Yang, D., *et al.*: Monai: An open-source framework for deep learning in healthcare. *arXiv preprint arXiv:2211.02701* (2022)
- [15] Diaz-Pinto, A., Alle, S., Nath, V., Tang, Y., Ihsani, A., Asad, M., Pérez-García, F., Mehta, P., Li, W., Flores, M., *et al.*: Monai label: A framework for ai-assisted interactive labeling of 3d medical images. *arXiv preprint arXiv:2203.12362* (2022)
- [16] Isensee, F., Jaeger, P.F., Kohl, S.A., Petersen, J., Maier-Hein, K.H.: nnu-net: a self-configuring method for deep learning-based biomedical image segmentation. *Nature methods* **18**(2), 203–211 (2021)

- [17] Johnson, A.E., Pollard, T.J., Greenbaum, N.R., Lungren, M.P., Deng, C.-y., Peng, Y., Lu, Z., Mark, R.G., Berkowitz, S.J., Horng, S.: Mimic-cxr-jpg, a large publicly available database of labeled chest radiographs. arXiv preprint arXiv:1901.07042 (2019)
- [18] Goldberger, A.L., Amaral, L.A., Glass, L., Hausdorff, J.M., Ivanov, P.C., Mark, R.G., Mietus, J.E., Moody, G.B., Peng, C.-K., Stanley, H.E.: Physiobank, physiotoolkit, and physionet: components of a new research resource for complex physiologic signals. *circulation* **101**(23), 215–220 (2000)
- [19] Landman, B., Xu, Z., Igelsias, J., Styner, M., Langerak, T., Klein, A.: Miccai multi-atlas labeling beyond the cranial vault—workshop and challenge. In: Proc. MICCAI Multi-Atlas Labeling Beyond Cranial Vault—Workshop Challenge, vol. 5, p. 12 (2015)
- [20] Kulkarni, P., Garin, S., Kanhere, A., Siegel, E., Yi, P.H., Parekh, V.S.: High-throughput ai inference for medical image classification and segmentation using intelligent streaming. arXiv preprint arXiv:2305.15617 (2023)
- [21] Kulkarni, P., Parekh, V.S.: Medical Image Streaming Toolkit (MIST). <https://github.com/UM2ii/MIST>
- [22] Kulkarni, P., Parekh, V.S.: Experiments for Medical Image Streaming Toolkit (MIST). https://github.com/UM2ii/MIST_Paper
- [23] Naman, A.: OpenJPH: Open source implementation of High-throughput JPEG2000 (HTJ2K). <https://github.com/aous72/OpenJPH>
- [24] Hafey, C.: openjphjs: JS/WebAssembly build of OpenJPH. <https://github.com/chafey/openjphjs>
- [25] Kulkarni, P.: openjphpy. <https://github.com/UM2ii/openjphpy>
- [26] Boliek, M., Christopoulos, C., Majani, E.: JPEG 2000 Image Coding System. <https://www.ics.uci.edu/~dan/class/267/papers/jpeg2000.pdf>
- [27] Wang, Z., Simoncelli, E.P., Bovik, A.C.: Multiscale structural similarity for image quality assessment. In: The Thirty-Seventh Asilomar Conference on Signals, Systems & Computers, 2003, vol. 2, pp. 1398–1402 (2003). Ieee
- [28] Huang, G., Liu, Z., Van Der Maaten, L., Weinberger, K.Q.: Densely connected convolutional networks. In: Proceedings of the IEEE Conference on Computer Vision and Pattern Recognition, pp. 4700–4708 (2017)
- [29] Çiçek, Ö., Abdulkadir, A., Lienkamp, S.S., Brox, T., Ronneberger, O.: 3d u-net: learning dense volumetric segmentation from sparse annotation. In: Medical Image Computing and Computer-Assisted Intervention—MICCAI 2016: 19th International Conference, Athens, Greece, October 17–21, 2016, Proceedings, Part II 19, pp. 424–432 (2016). Springer
- [30] LeCun, Y., Bottou, L., Orr, G.B., Müller, K.-R.: Efficient backprop. In: Neural Networks: Tricks of the Trade, pp. 9–50. Springer, ??? (2002)
- [31] Loshchilov, I., Hutter, F.: Sgdr: Stochastic gradient descent with warm restarts. arXiv preprint arXiv:1608.03983 (2016)